electronics

MDPI

Article

Progress in Violet Light-Emitting Diodes Based on ZnO/GaN Heterojunction

Roberto Macaluso [1], Giuseppe Lullo [1], Isodiana Crupi [1], Daniele Sciré [1], Fulvio Caruso [1,†], Eric Feltin [2] and Mauro Mosca [1,*]

1 Department of Engineering, University of Palermo, Viale delle Scienze, Building 9, I-90128 Palermo, Italy; roberto.macaluso@unipa.it (R.M.); giuseppe.lullo@unipa.it (G.L.); isodiana.crupi@unipa.it (I.C.); daniele.scire@unipa.it (D.S.); caruso.fulvio@gmail.com (F.C.)

2 Novagan LLC, EPFL Innovation Park, CH-1015 Lausanne, Switzerland; eric.feltin@novagan.com

* Correspondence: mauro.mosca@unipa.it; Tel.: +39-091-23860212

† F.C. is now with ABB Power Grids Switzerland Ltd., Semiconductors, CH-5600 Lenzburg, Switzerland.

Received: 7 May 2020; Accepted: 11 June 2020; Published: 13 June 2020

Abstract: Progress in light-emitting diodes (LEDs) based on ZnO/GaN heterojunctions has run into several obstacles during the last twenty years. While both the energy bandgap and lattice parameter of the two semiconductors are favorable to the development of such devices, other features related to the electrical and structural properties of the GaN layer prevent an efficient radiative recombination. This work illustrates some advances made on ZnO/GaN-based LEDs, by using high-thickness GaN layers for the *p*-region of the device and an ad hoc device topology. Heterojunction LEDs consist of a quasicoalesced non-intentionally doped ZnO nanorod layer deposited by chemical bath deposition onto a metal–organic vapor-phase epitaxy -grown epitaxial layer of *p*-doped GaN. Circular 200 µm-sized violet-emitting LEDs with a *p*-*n* contact distance as low as 3 µm exhibit a turn-on voltage of 3 V, and an emitting optical power at 395 nm of a few microwatts. Electroluminescence spectrum investigation shows that the emissive process can be ascribed to four different recombination transitions, dominated by the electron-hole recombinations on the ZnO side.

Keywords: ZnO/GaN heterojunction LEDs; ZnO nanorods; epitaxial *p*-GaN layers; chemical bath deposition; ZnO/GaN heterostructure

1. Introduction

ZnO is regarded as an attractive material for near-UV light-emitting diodes (LEDs) due to the wide direct bandgap (3.37 eV), the large exciton binding energy (60 meV), and several interesting optic and optoelectronic properties [1,2] which might allow for efficient near-bandgap recombination and laser working at room temperature [3]. ZnO is also considered, together with GaN, for the fabrication of both blue [4–7] and white LEDs, with and without any phosphor or dye [8–12]. Nevertheless, despite ample efforts to dope ZnO as a *p*-type semiconductor, reproducible and reliable *p*-type ZnO is not available, which prevents ZnO from being used in *p*-*n* homojunction LEDs [13]. The reasons for this failure are the low solubility of acceptor dopants [14], the height of the acceptor's level energy [15–18], and some self-compensating effects [19]. Furthermore, the results reported in the literature on ZnO-based homostructure LEDs are either not convincing or controversial, as reviewed in reference [20]. A different approach to ZnO homojunctions is the adoption of *n*-ZnO/*p*-GaN heterojunctions, since ZnO and GaN have the same wurtzite crystal structure with a low lattice-constant mismatch of 1.8%. Additionally, the bandgap energies of the two semiconductors are very close [21] and GaN exhibits a minor band offset with ZnO.

n-ZnO/*p*-GaN heterojunctions-based devices could take advantage of a strong excitonic emission if the radiative recombination occurred in the ZnO layer; nevertheless, many works report radiative recombination occurring mainly in the GaN side [5,7,22,23], due to the higher doping concentration of ZnO, generally higher than GaN.

The electroluminescence (EL) of LEDs based on *n*-ZnO/*p*-GaN heterojunctions strongly depends on the huge strain at the interface, which causes low quality heterojunctions [24]. Moreover, as well as a thin-film structure, the Fresnel coefficients and the total internal light reflections reduce the efficiency of light extraction [25]. These effects can be minimized if LEDs are fabricated in the form of ZnO nanorods on a GaN substrate. Nanoscale heterojunctions suffer less from strain at the interface, reducing misfit and threading dislocations [26]; likewise, light extraction is improved by using nanorods, which behave as waveguides [27,28].

In this work, we analyze more deeply how the optical power of heterojunction LEDs, grown as a dense collection of non-intentionally doped (*nid*) ZnO on a single layer of *p*-doped GaN, is influenced by both the device topology and the quality of the GaN layer. In particular, the distance between the *p*- and the *n*-contacts plays a key role in the efficiency of ZnO/GaN heterojunction LEDs. In a previous work [29], we proved that the recombination in the *n*-region depends on the spreading length of the holes coming from the *p*-contact; due to the poor conductivity of both the *p*-GaN and the *nid*-ZnO, the recombination occurs in the proximity of the edge of the *n*-contact. In particular, since the *p*-GaN is the base layer, hole injection would not occur along the vertical direction; the low conductivity of the ZnO does not allow the holes to spread for the full length of the *n*-pad. Consequently, to provide an efficient radiative recombination in the ZnO side of the junction, it is important to reduce to as low as possible the distance between the two contacts. Here, we report on optoelectronic properties, such as optical power, external quantum efficiency (EQE) and *I-V* characteristics of a *nid*-ZnO/*p*-GaN heterojunction LED with a contact distance as low as 3 µm, showing the improvement in the performances in relation to larger contact distances. It is worthwhile to point out that in almost all the papers concerning ZnO/GaN-based LEDs, very few groups have reported on the values of the optical power emitted by the devices and their EQE [30,31], probably because the performances of the devices were still too poor. This means that it is hard to evaluate and compare the real performance of these LEDs. Furthermore, in this work, the radiant power is studied against the GaN layer characteristics and a clear improvement of both hole transport and recombination features has been observed with a better quality of the GaN material.

A dense collection of *nid*-ZnO nanorods was deposited on *p*-GaN templates by chemical bath deposition (CBD). Two *p*-GaN layers with different thicknesses were tested in order to evaluate the influence of the quality of the *p*-type region on the carrier transport and the emitting properties of the devices. The emitted power, as well as the EQE, have been measured for 200 µm-sized and 3 µm-spacing between *p*- and *n*-contact LEDs.

2. Materials and Methods

Two substrates were used for this study: the first consisted of 1 µm-thick *p*-GaN grown onto 2 µm-thick *nid*-GaN (wafer A), while the second one was a (*p*-*n*)GaN structure, with only 100 nm of *p*-GaN, grown on a 1 µm-thick *n*-GaN (wafer B). All the GaN layers were grown by metal–organic vapor-phase epitaxy (MOVPE) on a 2 inch c-plane sapphire substrate in an AIXTRON 200/4 RF-S (AIXTRON, Herzogenrath, Germany) reactor, using triethylgallium (TEGa), ammonia (NH_3), and bis (cyclopentadienyl) magnesium (Cp_2Mg) as the metal–organic precursors for Ga, *N*, and Mg, respectively. Wafers A and B were provided by Novagan company (Lausanne, Switzerland). Epitaxial growth for the two samples was carried out according to the BKM (best known method) recipes developed for the AIXTRON 200/4 RF-S reactor. Both wafers were cut into small chips of approximately 1 cm^2 before being processed with direct laser writing lithography for both ZnO area definition and metal contacts patterning.

Bottom 100 nm-thick Cu contacts were patterned and deposited onto the *p*-GaN layer by thermal evaporation, then the regions to be covered with the ZnO nanorods were patterned and defined, and finally, 100 nm-thick Al contacts were deposited onto the grown ZnO nanorods. These ones are partially coalesced and behave as the *n*-region of the heterojunction. As a *p*-contact, we utilised Cu instead of standard Ni/Au or Pd/Au, since the latter ones required an annealing which could cause Zn ions to migrate towards the GaN layer [32]. Both Cu/p-GaN contact resistance and Schottky barrier height are close to those of Pd/p-GaN ones [33,34]. A layer of coalesced ZnO nanorods was preferred to a collection of isolated vertical nanorods with the empty gaps between them filled with an insulating supporting material like a polymer or spin-on-glass. In fact, since ZnO is known to exhibit piezophototronic effects, and the insertion of a supporting material between the nanorods could have modified the strain conditions and the radiative emission. A sketch of the devices is shown in Figure 1a.

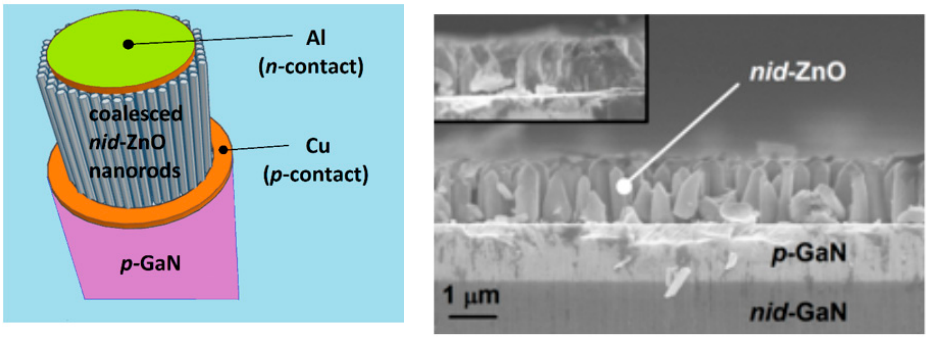

(**a**) (**b**)

Figure 1. (**a**) Sketch of the fabricated devices; (**b**) Cross-section scanning electron microscope (SEM) image of ZnO nanorods grown by chemical bath deposition (CBD) (3 h, 50 mM-concentrated nutrient solution) on wafer A. The inset shows a detail of the coalescence of the nanorods (the scale marker applies to both images).

ZnO nanorods were fabricated by CBD, which has been extensively illustrated in our previous papers [29,35,36]. The nutrient solution was prepared with zinc nitrate hexahydrate (Sigma-Aldrich, St. Louis, MO, USA, reagent grade 98%) and hexamethylenetetramine (Alfa Aesar, Ward Hill, MA, USA, ACS 99+%) in deionized water. The growth of the nanorods occurred at a temperature of 80 °C for 3 h.

X-ray diffraction (XRD) θ–2θ scan spectra were measured using a vertical goniometer with Cu K-α radiation (λ = 1.5405980 Å) over the 2θ range of 20°–90°.

Photoluminescence (PL) measurements were carried out by exciting the samples with the third harmonic of a Nd:YAG laser (355 nm). A light power-current-voltage (L-I-V) setup was used to measure the optical and electrical characteristics of the LEDs. The electroluminescence (EL) spectra were measured using an Ocean Optics (Edinburgh, Scotland, UK) HR4000CG UV–Vis spectrometer. Finally, an Ecopia (Anyang city, Gyeonggi-do, Korea) HMS-3000 Hall system (B = 0.55 T) provided carrier concentration and mobility measurements of the GaN layers.

3. Results and Discussion

The scanning electron microscope (SEM) image of Figure 1b shows the ZnO nanorods grown onto the wafer A. The nanorods appear to be dense and partially coalesced. The inset of Figure 1b shows that in several regions, the nanorods coalesce to form a compact layer. The high density can be ascribed to the high concentration of the nutrient solution [37–39]. The thickness of the ZnO nanorods (referred as the *nid*-ZnO layer) is approximately equal to 1 µm and depends on the CBD process duration,

as demonstrated in a previous work [40]. A dense nanorods layer allows easier handling during the subsequent metal contacts fabrication and does not require further processing steps.

Figure 2 shows the XRD diffractogram of ZnO rods grown on wafer A. The strong diffraction peaks, located at 34.43° and 72.74°, are in good agreement with those reported for ZnO (002) and ZnO (004), respectively, in JCPDS # 36-1451. This result confirms that the CBD technique leads to wurtzite nanostructures with a pronounced vertical orientation.

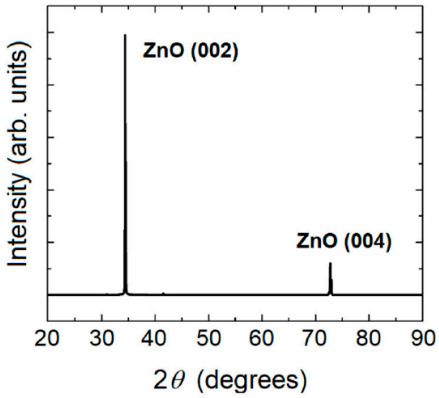

Figure 2. X-ray diffraction (XRD) diffractogram of ZnO nanorods grown on wafer A.

As reported in reference [29], the conductivity of the *p*-GaN layer is of crucial importance to have an efficient hole injection in the *n*-region. A low current injection results in both a poor light emission performance and a high turn-on voltage. The conductivity of the *p*-layer does not only depend on the hole concentration but also on the hole mobility. Therefore, a better crystalline quality of the *p*-GaN layer can increase the emitted power and improve the EQE.

Figure 3 exhibits the optical power emitted at 9 V of several different size circular LEDs (100 μm, 200 μm, and 400 μm) fabricated by using both wafer A and B. The distance between *n*- and *p*-contacts is 20 μm. The better quality of the *p*-GaN layer of wafer A, due to its larger thickness, leads to higher optical power and, in general, to better LED performances. Therefore, in ZnO/GaN heterojunction LEDs, particular care should be taken to use *p*-GaN templates of high-crystalline quality, not only to improve the hole injection in the *n*-region, but also to guarantee an efficient light emission. It is worth pointing out that the optical power poorly depends on LED size, given that the recombination region is limited by the hole spreading length which is lower than the LED size [29].

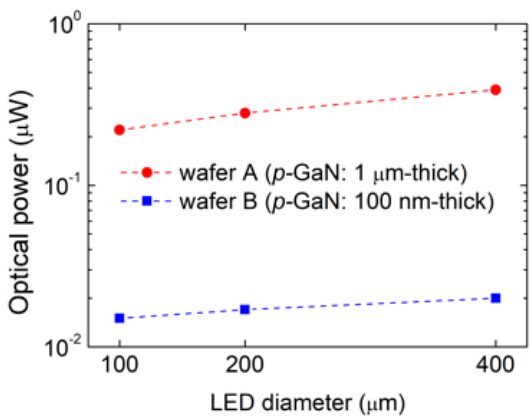

Figure 3. Optical power emitted at 9 V for light-emitting diodes (LED) fabricated on wafer A and wafer B as a function of LED size. The distance between *n*- and *p*-contacts is 20 μm. The dashed line serves as a guide for the eye.

Figure 4a presents the PL spectra of *p*-GaN and *nid*-ZnO (wafer A). The first one exhibits a broad emission band between 360 nm and 375 nm, whereas the second one a narrower peak centered at 390 nm. Most of papers report *p*-GaN PL peaks centered between 430 nm and 450 nm [5,30,41–45], these higher values depending on the high concentration of Mg in GaN (generally larger than 10^{18} cm^{-3}). Our *p*-GaN template (wafer A) exhibits instead an acceptor concentration as low as 2.5×10^{16} cm^{-3} and a carrier mobility of 60 cm^2/(Vs), as assessed by Hall measurements.

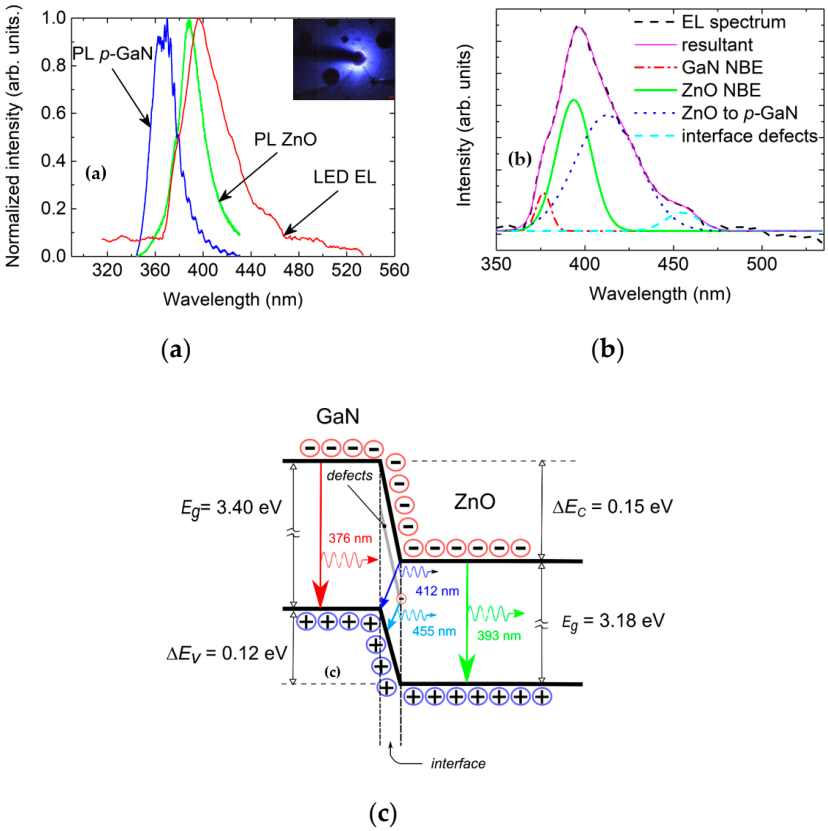

Figure 4. (**a**) PL spectra of *p*-GaN and *nid*-ZnO (wafer A) and EL spectrum of a 200 µm-sized LED at 50 mA fabricated on wafer A. Fluctuations in the p-GaN PL spectrum are due to Fabry–Perot effects. Inset: photo of the LED biased at 20 mA; (**b**) Peak deconvolution of the EL spectrum with Gaussian functions: peaks centered respectively at 376 nm, corresponding to GaN near band-edge (NBE) emission; 393 nm, corresponding to ZnO NBE emission; 412 nm, corresponding to the electron injection from the conduction band of the ZnO to the acceptor levels of the GaN; 455 nm, corresponding to radiative defect recombination at the interface. In the magenta solid line is reported the resultant fitting spectrum; (**c**) Band diagram of *nid*-ZnO/*p*-GaN heterojunction with the transitions indicated by arrows.

Concerning the ZnO PL spectrum, the ZnO nanorod layer presents a lower bandgap energy (E_g = 3.18 eV) than in bulk form (estimated as E_g = 3.37 eV [1]), owing to the shifting of the valence band maximum and conduction band minimum of ZnO when prepared using a wet chemistry method [46]. Other factors that can modify the bandgap of ZnO nanorods are: growth time [47,48], aspect ratio [49], and substrate [50]. The value of E_g = 3.18 eV for our ZnO nanorod layer is in agreement with the values reported in the literature [47,48]. The full width at half maximum (FWHM) of the ZnO PL peak is 25 nm, comparable with values obtained in epitaxial ZnO [51]. This narrow peak indicates the high quality of ZnO nanorods grown by CBD.

Figure 4a also shows the EL spectrum of a 200 µm-sized LED, fabricated on wafer A and working at 50 mA. The EL spectrum consists of a dominant violet emission peak centered at 395 nm (a photo of an LED biased at 20 mA is shown in the inset of Figure 4a), due to ZnO near band-edge (NBE) emission,

and other wavelength components which notably increase with the injection current. However, the position of the EL peak does not appreciably shift with the current. No other peaks or bands are found in the visible range, proving the excellent quality of the materials. By comparing the EL spectrum with the PL spectra of the ZnO (emission peak centered at 390 nm) and the *p*-GaN (broad emission centered at 365 nm), it is possible to infer that the violet emission could be mainly ascribed to carrier recombination from the conduction band (or shallow donor levels induced by native defects) to the valence band in the ZnO layer. Furthermore, since for a *p*-*n* junction $N_A W_P = N_D W_n$ (with N_A and N_D concentration of acceptors and donors, respectively, and W_p and W_n width of the depletion region in the *p*- and *n*-side, respectively), a low density of donors in the ZnO region (which is non-intentionally doped) leads to a large ZnO depletion region.

A more accurate analysis is carried out in Figure 4b by peak deconvolution of the EL spectrum with Gaussian functions centered at 376 nm, 393 nm, 412 nm, and 455 nm, attributed to four different processes to be identified. The highest peak located at 393 nm corresponds to the predominant mechanism of recombination, that is, the recombination of the free excitons in ZnO (near band-edge emission). The ultraviolet emission at 376 nm is attributed to transition recombination in *p*-GaN, as observed in the PL spectrum reported in Figure 4b. The small intensity of the peak confirms that recombination does mainly occur in the ZnO side of the junction. The blue peak at 412 nm could be ascribed to the electron injection from the conduction band of the ZnO to the valence band of the GaN (radiative interfacial recombination) [6,44]. At the interface, the gap (ZnO side) is equal to the ZnO bandgap minus the valence band offsets ($E_{g(\mathrm{ZnO})} - E_V = 3.18 - 0.12 = 3.06$ eV). The red shift between PL and EL peaks is attributed to different bias conditions during measurements. The origin of the last peak at 455 nm is uncertain: probably, as suggested in reference [6], the emission originates in defect transitions at the ZnO/GaN interface. Another hypothesis is that this peak could be ascribed to ZnO neutral oxygen vacancy (V_O^X) defect-related recombination (corresponding to a 2.74 eV transition) [52]. Nevertheless, the peak is not observed in the ZnO PL spectrum, suggesting that the transition is rather localized far from the surface, in correspondence to the heterojunction. Consequently, a band of interfacial defects due to the small lattice mismatch existing at the GaN/ZnO interface seems to be responsible for the peak at 455 nm. Figure 4c shows the band diagram of the *nid*-ZnO/*p*-GaN heterostructure with the involved radiative recombination processes.

Figure 5 shows respectively: (a) direct- and reverse-biased *I*-*V* characteristics, (b) optical power and EQE as a function of current, for a circular 200 μm-sized LED fabricated on wafer A. In order to maximize the injection of the carriers, the distance *d* between the *p*- and *n*-contacts was reduced to 3 μm. As a term of comparison, optical power vs. current is also shown for an LED with *d* = 20 μm.

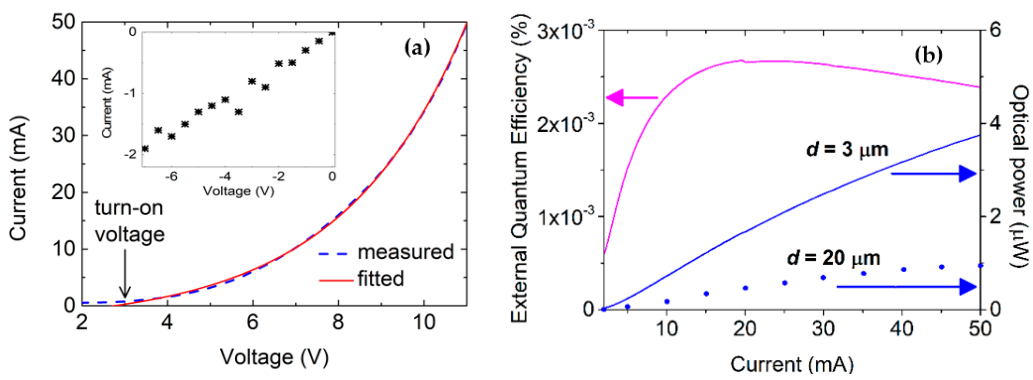

Figure 5. (**a**) Experimentally measured *I*-*V* data (dashed line) and exponential data fitting (solid line) for a 200 μm-sized LED grown on wafer A. The inset shows the reverse *I*-*V* characteristic; (**b**) Optical power and external quantum efficiency as a function of current for a 200 μm-sized LED grown on wafer A. The distance *d* between *p*- and *n*-contacts equals 3 μm, except for the dotted curve in Figure 5b, which is related to an LED with *d* = 20 μm grown on wafer A.

The turn-on voltage is around 3 V, in good agreement with the best results found in the literature [53–55]. At 10 mA, the voltage is around 7 V. The reverse characteristic in the inset of Figure 5a is roughly linear and shows leakage currents (−1.9 mA at −7 V), since the device is not optimized; nevertheless, the *I-V* data (dashed curve) well fit with an exponential *p-n* junction model (solid curve). Clearly, the model deviates from data at low voltage bias (lower than turn-on voltage) due to the leakage effects. The emitted power is of the order of microwatts, while the maximum of the EQE is 2.7×10^{-3}%. Due to the reduction in the distance between the contacts, the optical power values show a significant enhancement (by approximately a factor of 4 compared to a 200 µm LED on wafer A with 20 µm of contact distance).

Additional improvements of the emissive performances of the devices could be obtained by extrinsic doping of the ZnO region (with Al, for example) and further improving of its crystalline structure. Furthermore, a more compact structure would lead to a reduced current leakage and improved EQE.

4. Conclusions

This work reports on some improvements in *nid*-ZnO/*p*-GaN heterojunction LEDs fabricated, taking special care both in the choice of the *p*-GaN layer thickness and in the design of the structure layout. Electrical and optical characteristics of the LEDs are presented and discussed. In particular, results show the strong dependence of the radiative recombination of the devices on the distance between the *p*- and the *n*-contacts. For a circular 200 µm-sized LED and a 3 µm-gap between the *p*- and *n*-contacts, a turn-on voltage of 3 V, an emitting optical power of a few microwatts, and a maximum of the EQE of 2.7×10^{-3}% are measured. While the device is not optimized, the reduced spacing between the contacts provides an improved emission performance. The EL spectrum at room temperature shows a main peak at 395 nm, primarily due to the holes injected into the *n* region and the recombination process from the conduction band to the valence band in the ZnO layer.

Author Contributions: Conceptualization, M.M. and F.C.; methodology, M.M., R.M., F.C., G.L., E.F., and I.C.; software, M.M., R.M., D.S., and G.L.; validation, M.M., R.M., and I.C.; formal analysis, M.M., R.M., and G.L.; investigation, D.S. and F.C.; resources, E.F. and G.L.; data curation, R.M., D.S., and I.C.; writing—original draft preparation, M.M.; writing—review and editing, M.M., R.M., F.C., D.S., and I.C.; visualization, I.C., R.M., and G.L.; supervision, M.M.; project administration, M.M.; funding acquisition, M.M., R.M., and I.C. All authors have read and agreed to the published version of the manuscript.

Funding: This research received no external funding.

Conflicts of Interest: The authors declare no conflict of interest.

References

1. Morkoç, H.; Özgür, Ü. *Zinc Oxide: Fundamentals, Materials and Device Technology*; Wiley-VCH: Weinheim, Germany, 2009; ISBN 978-3-527-40813-9.
2. Boughelout, A.; Zebbar, N.; Macaluso, R.; Zohour, Z.; Bensouilah, A.; Zaffora, A.; Aida, M.S.; Kechouane, M.; Trari, M. Rhodamine (B) photocatalysis under solar light on high crystalline ZnO films grown by home-made DC sputtering. *Optik* **2018**, *174*, 77–85. [CrossRef]
3. Janotti, A.; van de Walle, C.G. Fundamentals of zinc oxide as a semiconductor. *Rep. Prog. Phys.* **2009**, *72*, 126501. [CrossRef]
4. Hassan, J.J.; Mahdi, M.A.; Yusof, Y.; Abu-Hassan, H.; Hassan, Z.; Al-Attar, H.A.; Monkman, A.P. Fabrication of ZnO nanorod/p-GaN high-brightness UV LED by microwave-assisted chemical bath deposition with Zn(OH)2–PVA nanocomposites as seed layer. *Opt. Mater.* **2013**, *35*, 1035–1041. [CrossRef]
5. Ko, R.M.; Wang, S.J.; Chen, C.Y.; Wu, C.H.; Lin, Y.R.; Lo, H.M. Hydrothermal growth of n-ZnO films on a patterned p-GaN epilayer and its application in heterojunction light-emitting diodes. *Jpn. J. Appl. Phys.* **2017**, *56*, 04CH03. [CrossRef]
6. Jha, S.K.; Kutsay, O.; Bello, I.; Lee, S.T. ZnO nanorod based low turn-on voltage LEDs with wide electroluminescence spectra. *J. Lumin.* **2013**, *133*, 222–225. [CrossRef]

7. Alivov, Y.I.; van Nostrand, J.E.; Look, D.C.; Chukichev, M.V.; Ataev, B.M. Observation of 430 nm electroluminescence from ZnO/GaN heterojunction light-emitting diodes. *Appl. Phys. Lett.* **2003**, *83*, 2943–2945. [CrossRef]
8. Sadaf, J.R.; Israr, M.Q.; Kishwar, S.; Nur, O.; Willander, M. Forward and reverse-biased electroluminescence behavior of chemically fabricated ZnO nanotubes/GaN interface. *Semicond. Sci. Technol.* **2011**, *26*, 075003. [CrossRef]
9. Park, G.C.; Hwang, S.M.; Lee, S.M.; Choi, J.H.; Song, K.M.; Kim, H.Y.; Kim, H.S.; Eum, S.J.; Jung, S.B.; Lim, J.H.; et al. Hydrothermally Grown In-doped ZnO Nanorods on p-GaN Films for Color-tunable Heterojunction Light-emitting-diodes. *Sci. Rep.* **2015**, *5*. [CrossRef]
10. Huo, C.; Lu, Y.; Zeng, H.; Cao, P.; Han, S.; Liu, W.; Jia, F.; Zeng, Y.; Liu, X.; Xu, W.; et al. Facile approaches to prepare n-ZnO/(i-ZnO)/p-GaN heterojunction light-emitting diodes with white-light-electroluminescence. *Appl. Phys. Express* **2019**, *12*, 121004. [CrossRef]
11. Caruso, F.; Mosca, M.; Rinella, S.; Macaluso, R.; Calì, C.; Saiano, F.; Feltin, E. Frequency-Downconversion Stability of PMMA Coatings in Hybrid White Light-Emitting Diodes. *J. Electron. Mater.* **2016**, *45*, 682–687. [CrossRef]
12. Mosca, M.; Caruso, F.; Zambito, L.; Seminara, B.; Macaluso, R.; Calì, C.; Feltin, E. *Warm white LED Light by Frequency Down-conversion of Mixed Yellow and Red Lumogen*; Fédéli, J.-M., Vivien, L., Smit, M.K., Eds.; International Society for Optics and Photonics: Grenoble, France, 2013; p. 87670L.
13. Look, D.C. Electrical and optical properties of p-type ZnO. *Semicond. Sci. Technol.* **2005**, *20*, S55–S61. [CrossRef]
14. Limpijumnong, S.; Gordon, L.; Miao, M.; Janotti, A.; van de Walle, C.G. Alternative sources of p-type conduction in acceptor-doped ZnO. *Appl. Phys. Lett.* **2010**, *97*, 072112. [CrossRef]
15. Yan, Y.; Al-Jassim, M.M.; Wei, S.H. Doping of ZnO by group-IB elements. *Appl. Phys. Lett.* **2006**, *89*, 181912. [CrossRef]
16. Park, C.H.; Zhang, S.B.; Wei, S.H. Origin of *p* -type doping difficulty in ZnO: The impurity perspective. *Phys. Rev. B* **2002**, *66*, 073202. [CrossRef]
17. Lyons, J.L.; Janotti, A.; van de Walle, C.G. Why nitrogen cannot lead to p-type conductivity in ZnO. *Appl. Phys. Lett.* **2009**, *95*, 252105. [CrossRef]
18. Tarun, M.C.; Iqbal, M.Z.; McCluskey, M.D. Nitrogen is a deep acceptor in ZnO. *AIP Adv.* **2011**, *1*, 022105. [CrossRef]
19. Avrutin, V.; Silversmith, D.J.; Morkoç, H. Doping Asymmetry Problem in ZnO: Current Status and Outlook. *Proc. IEEE* **2010**, *98*, 1269–1280. [CrossRef]
20. Mosca, M.; Macaluso, R.; Caruso, F.; Lo Muzzo, V.; Calì, C. The p-type doping of ZnO: Mirage or reality? In *Advances in Semiconductor Research: Physics of Nanosystems, Spintronics and Technological Applications*; Adorno, D.P., Pokutnyi, S., Eds.; Physics Research and Technolog: New York, NY, USA, 2015; pp. 245–282. ISBN 978-1-63321-755-3.
21. Vispute, R.D.; Talyansky, V.; Choopun, S.; Sharma, R.P.; Venkatesan, T.; He, M.; Tang, X.; Halpern, J.B.; Spencer, M.G.; Li, Y.X.; et al. Heteroepitaxy of ZnO on GaN and its implications for fabrication of hybrid optoelectronic devices. *Appl. Phys. Lett.* **1998**, *73*, 348–350. [CrossRef]
22. Shen, Y.; Chen, X.; Yan, X.; Yi, F.; Bai, Z.; Zheng, X.; Lin, P.; Zhang, Y. Low-voltage blue light emission from n-ZnO/p-GaN heterojunction formed by RF magnetron sputtering method. *Curr. Appl. Phys.* **2014**, *14*, 345–348. [CrossRef]
23. Fu, Q.M.; Cao, W.; Li, G.W.; Lin, Z.D.; Chen, Z.; Xu, C.B.; Tu, Y.F.; Ma, Z.-B. Blue/green electroluminescence from a ZnO nanorods/p-GaN heterojunction light emitting diode under different reverse bias. *Appl. Surf. Sci.* **2014**, *293*, 225–228. [CrossRef]
24. Gruber, T.; Kirchner, C.; Thonke, K.; Sauer, R.; Waag, A. MOCVD Growth of ZnO for Optoelectronic Applications. *Phys. Status Solidi A* **2002**, *192*, 166–170. [CrossRef]
25. Hsiao, Y.H.; Chen, C.Y.; Huang, L.C.; Lin, G.J.; Lien, D.H.; Huang, J.J.; He, J.H. Light extraction enhancement with radiation pattern shaping of LEDs by waveguiding nanorods with impedance-matching tips. *Nanoscale* **2014**, *6*, 2624–2628. [CrossRef] [PubMed]
26. Klingshirn, C.F.; Meyer, B.K.; Waag, A.; Hoffmann, A.; Geurts, J. *Zinc Oxide: From Fundamental Properties Towards Novel Applications*; Springer: Berlin/Heidelberg, Germany, 2010; ISBN 978-3-642-10576-0.

27. Xu, S.; Xu, C.; Liu, Y.; Hu, Y.; Yang, R.; Yang, Q.; Ryou, J.H.; Kim, H.J.; Lochner, Z.; Choi, S.; et al. Ordered Nanowire Array Blue/Near-UV Light Emitting Diodes. *Adv. Mater.* **2010**, *22*, 4749–4753. [CrossRef] [PubMed]
28. Shi, Z.; Zhang, Y.; Cui, X.; Wu, B.; Zhuang, S.; Yang, F.; Yang, X.; Zhang, B.; Du, G. Improvement of electroluminescence performance by integration of ZnO nanowires and single-crystalline films on ZnO/GaN heterojunction. *Appl. Phys. Lett.* **2014**, *104*, 131109. [CrossRef]
29. Macaluso, R.; Lullo, G.; Crupi, I.; Caruso, F.; Feltin, E.; Mosca, M. Current Spreading Length and Injection Efficiency in ZnO/GaN-Based Light-Emitting Diodes. *IEEE Trans. Electron. Devices* **2019**, *66*, 4811–4816. [CrossRef]
30. Rogers, D.J.; Teherani, F.H.; Yasan, A.; Minder, K.; Kung, P.; Razeghi, M. Electroluminescence at 375nm from a ZnO/GaN:Mg/c-Al2O3 heterojunction light emitting diode. *Appl. Phys. Lett.* **2006**, *88*, 141918. [CrossRef]
31. Bano, N.; Hussain, I.; Sawaf, S.; Alshammari, A.; Saleemi, F. Enhancement of external quantum efficiency and quality of heterojunction white LEDs by varying the size of ZnO nanorods. *Nanotechnology* **2017**, *28*, 245203. [CrossRef]
32. Macaluso, R.; Mosca, M.; Calì, C.; Di Franco, F.; Santamaria, M.; Di Quarto, F.; Reverchon, J.L. Erroneous *p* -type assignment by Hall effect measurements in annealed ZnO films grown on InP substrate. *J. Appl. Phys.* **2013**, *113*, 164508. [CrossRef]
33. Koide, Y.; Ishikawa, H.; Kobayashi, S.; Yamasaki, S.; Nagai, S.; Umezaki, J.; Koike, M.; Murakami, M. Dependence of electrical properties on work functions of metals contacting to p-type GaN. *Appl. Surf. Sci.* **1997**, *117–118*, 373–379. [CrossRef]
34. Park, Y.; Ahn, K.S.; Kim, H. Schottky Barrier Height and S-Parameter of Ti, Cu, Pd, and Pt Contacts on p-Type GaN. *Jpn. J. Appl. Phys.* **2012**, *51*, 09MK01. [CrossRef]
35. Caruso, F.; Mosca, M.; Macaluso, R.; Cali, C.; Feltin, E. Well-aligned hydrothermally synthesized zinc oxide nanorods on p-gan without a seed layer. In Proceedings of the 2015 IEEE 15th International Conference on Nanotechnology (IEEE-NANO), Rome, Italy, 27–30 July 2015; pp. 1012–1014.
36. Barbagiovanni, E.G.; Strano, V.; Franzò, G.; Crupi, I.; Mirabella, S. Photoluminescence transient study of surface defects in ZnO nanorods grown by chemical bath deposition. *Appl. Phys. Lett.* **2015**, *106*, 093108. [CrossRef]
37. Jing, W.; Qi, H.; Shi, J.; Jiang, Z.; Zhou, F.; Cheng, Y.; Gao, K. Effects of the geometries of micro-scale substrates on the surface morphologies of ZnO nanorod-based hierarchical structures. *Appl. Surf. Sci.* **2015**, *355*, 403–410. [CrossRef]
38. Guo, M.; Diao, P.; Cai, S. Hydrothermal growth of well-aligned ZnO nanorod arrays: Dependence of morphology and alignment ordering upon preparing conditions. *J. Solid State Chem.* **2005**, *178*, 1864–1873. [CrossRef]
39. Zhang, S.; Wang, Y.; Ren, F.; Feng, T.; Wan, R.; Zhao, S.; Liang, M.; Wang, J.; Li, J.; Liu, Z.; et al. Systematic study of vertically aligned ZnO nanowire arrays synthesized on p-GaN substrate by hydrothermal method. *Jpn. J. Appl. Phys.* **2020**, *59*, 015503. [CrossRef]
40. Mosca, M.; Crupi, I.; Russotto, D.C.; Lullo, G.; Macaluso, R.; Giaconia, C.G.; Mirabella, S.; Feltin, E. Chemical Bath Deposition as a Simple Way to Grow Isolated and Coalesced ZnO Nanorods for Light-Emitting Diodes Fabrication. In Proceedings of the 2018 IEEE 4th International Forum on Research and Technology for Society and Industry (RTSI), Palermo, Italy, 10–13 September 2018; pp. 1–6.
41. Jeong, S.; Kim, H. Carrier transport analysis of n-ZnO:Al/p-GaN:Mg heterojunction light-emitting diodes. *J. Vac. Sci. Technol. B* **2015**, *33*, 021205. [CrossRef]
42. Jiang, J.; Zhang, Y.; Chi, C.; Shi, Z.; Yan, L.; Li, P.; Zhang, B.; Du, G. Improved ultraviolet emission performance from polarization-engineered n-ZnO/p-GaN heterojunction diode. *Appl. Phys. Lett.* **2016**, *108*, 063505. [CrossRef]
43. Lee, S.D.; Kim, Y.S.; Yi, M.S.; Choi, J.Y.; Kim, S.W. Morphology Control and Electroluminescence of ZnO Nanorod/GaN Heterojunctions Prepared Using Aqueous Solution. *J. Phys. Chem. C* **2009**, *113*, 8954–8958. [CrossRef]
44. Chen, C.; Zhang, J.; Chen, J.; Wang, S.; Liang, R.; Zhang, W.; Dai, J.; Chen, C. Near-ultraviolet electroluminescence from ZnO-based light-emitting diodes with n-ZnO nanorod/p-GaN direct-bonding heterojunction structure. *Mater. Lett.* **2017**, *189*, 144–147. [CrossRef]

45. Mo, X.; Fang, G.; Long, H.; Li, S.; Huang, H.; Wang, H.; Liu, Y.; Meng, X.; Zhang, Y.; Pan, C. Near-ultraviolet light-emitting diodes realized from n-ZnO nanorod/p-GaN direct-bonding heterostructures. *J. Lumin.* **2013**, *137*, 116–120. [CrossRef]
46. Kamarulzaman, N.; Kasim, M.F.; Rusdi, R. Band Gap Narrowing and Widening of ZnO Nanostructures and Doped Materials. *Nanoscale Res. Lett.* **2015**, *10*, 346. [CrossRef]
47. Idiawati, R.; Mufti, N.; Taufiq, A.; Wisodo, H.; Laila, I.K.R.; Fuad, A. Sunaryono Effect of Growth Time on the Characteristics of ZnO Nanorods. *IOP Conf. Ser.: Mater. Sci. Eng.* **2017**, *202*, 012050. [CrossRef]
48. Abdulrahman, A.F.; Ahmed, S.M.; Almessiere, M.A. Effect Of The Growth Time On The Optical Properties Of Zno Nanorods Grown By Low Temperature Method. *Dig. J. Nanomater. Biostruct.* **2017**, *12*, 1001–1009.
49. Kasim, M.F.; Kamarulzaman, N.; Rusdi, R. Effect of the Diameter on the Band Gap of ZnO Nanorods. *ECS Meet. Abstr.* **2014**, *MA2014-02*, 2095. [CrossRef]
50. Sáenz-Trevizo, A.; Amézaga-Madrid, P.; Pizá-Ruiz, P.; Antúnez-Flores, W.; Miki-Yoshida, M. Optical Band Gap Estimation of ZnO Nanorods. *Mat. Res.* **2016**, *19*, 33–38. [CrossRef]
51. Kashiwaba, Y.; Haga, K.; Watanabe, H.; Zhang, B.P.; Segawa, Y.; Wakatsuki, K. Structures and Photoluminescence Properties of ZnO Films Epitaxially Grown by Atmospheric Pressure MOCVD. *Phys. Status Solidi B Basic Res.* **2002**, *229*, 921–924. [CrossRef]
52. Jiang, H.; Lu, Y.; Rong, X.; Han, S.; Cao, P.; Zeng, Y.; Xu, W.; Fang, M.; Liu, W.; Zhu, D. Electroluminescence Properties of a Zinc Oxide Nanorod Array Heterojunction Light-Emitting Diode. *J. Electron. Mater.* **2020**. [CrossRef]
53. Yu, C.; Li, R.; Li, T.; Dong, H.; Jia, W.; Xu, B. Effect of Indium doping on the photoelectric properties of n-ZnO nanorods/p-GaN heterojunction light-emitting diodes. *Superlattice Microst.* **2018**, *120*, 298–304. [CrossRef]
54. Jeong, S.; Oh, S.K.; Ryou, J.H.; Ahn, K.S.; Song, K.M.; Kim, H. Monolithic Inorganic ZnO/GaN Semiconductors Heterojunction White Light-Emitting Diodes. *ACS Appl. Mater. Interfaces* **2018**, *10*, 3761–3768. [CrossRef]
55. Li, L.; Zhang, Y.; Yan, L.; Jiang, J.; Han, X.; Deng, G.; Chi, C.; Song, J. n-ZnO/p-GaN heterojunction light-emitting diodes featuring a buried polarization-induced tunneling junction. *AIP Adv.* **2016**, *6*, 125204. [CrossRef]